

DC Link Harmonics of Three Phase Voltage Source Converters Influenced by the Pulse Width Modulation Strategy – an Analysis

Michael Bierhoff

Chair for Power Electronics and Electrical Drives
Christian-Albrechts-University of Kiel
Kaiserstr. 2, 24143 Kiel
Germany
mib@tf.uni-kiel.de

Friedrich W. Fuchs

Chair for Power Electronics and Electrical Drives
Christian-Albrechts-University of Kiel
Kaiserstr. 2, 24143 Kiel
Germany
fwf@tf.uni-kiel.de

Abstract—Dc link current harmonics are the predominant factor to be considered for dimensioning dc capacitors in three phase PWM voltage source converters. In this article an analysis of the dc link current harmonics applying double Fourier series is derived. The analytical results for the dc link current spectra of continuous and discontinuous PWM are presented and compared with measurement results taken from a converter test setup. A good match between theoretically expected and actually obtained experimental results can be stated. Moreover significant differences between the investigated modulation strategies regarding their dc link current spectra can be found.

I. INTRODUCTION

Nowadays PWM voltage source converters constitute the most important means to control adjustable speed drives or generally to serve as an active rectifier with low effects to the mains. An appropriate design of their power section has to be done including the dc link capacitor. The capacitor sizing basically aims two issues, dc ripple voltage and more important capacitor lifetime which can directly be linked to its power losses. These subjects are affected in particular by the capacitor currents which coincide with the dc current harmonics in steady state operation under certain presumptions.

There are already several articles on the calculation of the RMS value of the dc link ripple current [1]–[3] which eventually all lead to the same results regardless of the modulation strategy. This value is only affected by the duty cycles of the active space vectors and thus it will be of the same quantity for all modulation waveforms as long as only one converter is considered to be the source of harmonics on the dc bus. Another numerical approach is presented in [4] where the interference of two different PWM converters connected to the same dc bus is examined. There it turns out that the phase shift of the respective switching periods would have an effect on the dc bus ripple current. However using different modulation strategies or switching frequencies as applied only to a single converter does not influence the dc link ripple current but the dispersion of the dc link current spectra. Hence the dc link current spectrum has to be analyzed for any applied modulation method to predict resulting capacitor ripple voltage for instance.

As the dc link capacitor constitutes an integrating filter on the dc link current a change of the modulation strategy and thus of the current spectra leads to a change of the ripple voltage. This inherently can be seen in [2] where different modulation methods are compared analytically but only in time domain.

Regarding the aging of the capacitor, its heating and thus power losses have to be taken into account. These power losses are a function of the capacitor current and its

series resistance. Usually the RMS value of the dc link current is used for the design but since the series resistance of a capacitor $ESR(\omega)$ shows some dependency on the frequency [5], [6] for detailed design it might be necessary to determine the capacitor current spectra explicitly. The dc current spectrum already has been calculated and measured for sine triangular modulation in [3] and determined by experiment for space vector modulation as well [5].

This work contributes a comprehensive analytical approach to determine the dc bus current spectra explicitly for any kind of modulation strategy, thereby utilizing the double Fourier series introduced in [7]. This approach has been already applied successfully for the harmonics calculation of the three phase currents of PWM voltage source converters as reported by various sources [8], [9].

In section II of this article the principles of pulse width modulation are pointed out which will be important for the analysis. Section III covers the derivation of the double Fourier series according to Black and determination of the dc bus harmonics. Computed results compared with experimental ones are presented in section IV that is followed by a conclusion.

II. PRINCIPLES OF PULSE WIDTH MODULATION

Basis for the analysis is a converter topology as shown by fig. 1 operated with pulse width modulation. Fig. 2 depicts the corresponding pulse scheme for switches $V_1 - V_3$ during an exemplary switching period. Involving these switches only into consideration is sufficient since the dc link current $i_{d,conv}$ can be composed of the switched currents $i_{V1} - i_{V3}$. For this example the instantaneous voltage command space vector is located in the first sector of the vector space that is spanned by the six possible switching states of the basic space vectors. It is well known that the command space vector resembles the sliding mean value of switched basic space vectors $\underline{V}_1, \underline{V}_2$ and $\underline{V}_0, \underline{V}_7$ being turned on for the time period t_1, t_2, t_0 and t_7 respectively during the switching period T_s [9]. These space vectors in turn correspond to specific switching combinations of the six semiconductor switches, see fig. 2. During the time period t_0 all upper switches (fig. 1) are

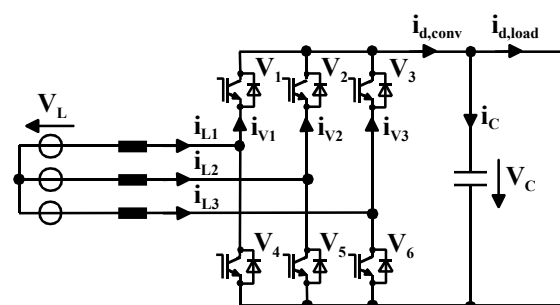


Figure 1. Three phase voltage source converter topology

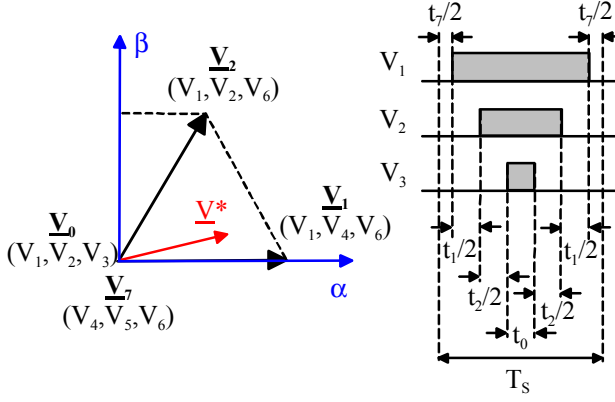


Figure 2. Switching scheme for upper bridge valves in the first sector of the complex plane

turned on whereas during t_7 only the lower ones are turned on. However during both time periods t_0 and t_7 the ac load is short circuited and the dc bus current flow is interrupted. While the switches are turned on the switch currents match the corresponding line currents. Hence during time period t_1 the instantaneous value of line current i_{L1} determines the dc bus current and during time span t_2 the dc bus current equals the sum of currents $i_{L1} + i_{L2}$. For the presented analysis the line currents are assumed to be purely sinusoidal.

The presented calculus is derived by considering carrier based PWM. In [9] - [11] the direct relation between space vector and naturally sampled carrier based PWM is explained. These relations yield the conclusion that the carrier function that would be applied according to fig. 2 is a triangular function which can be deduced from the symmetrical arrangement of switching duty cycles. Moreover with this analogy the switching period T_s would be equal to the carrier function period of a comparable carrier based PWM. The corresponding modulation waveform is determined by the duty cycles of the two different zero space vectors.

III. DC LINK CURRENT SPECTRA DESCRIBED BY DOUBLE FOURIER SERIES

A. The Geometric Wall Model

In general the determination of the analytical spectra of pulse width modulated values is a tedious issue. Even if solved, the appropriate equations yield infinite series comprising complex terms. One approach to determine the dc link current spectra analytically is given by [3]. The standard approach utilizing the geometric wall model [7] resulting in double Fourier series is presented here. This method provides a fairly simple way to obtain expressions for the Fourier coefficients of line side or dc side current harmonics generated by any modulation strategy.

Initially the geometric wall model was applied for the analysis of asynchronous sinusoidal modulation schemes to overcome the problems caused by non periodic behaviour of the pulse waveform [8]. A plain view for the actually three dimensional considered model is given by fig. 3. The 'walls' are represented by the boundaries of the shaded areas with an original height of the dc link voltage V_{dc} [8], [9]. The important modification to apply this method on the dc current is to adjust the height of the walls to the instantaneous value of the line current $i_L(\omega t)$. The walls are oriented perpendicular to the x-y plane. The

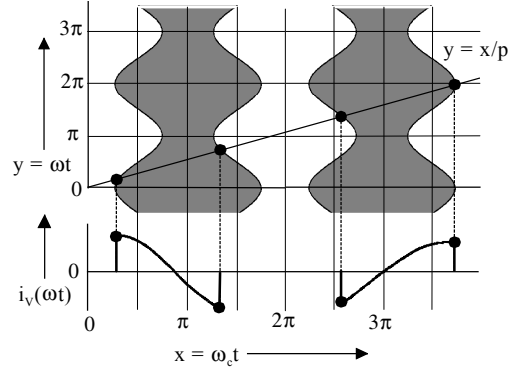


Figure 3. The geometric wall model as applied on a cosine modulation function in combination with a triangular carrier

assumption of unipolar switching introduces an erroneous dc component when the line voltage harmonics are regarded [8]. But since the resulting pulse widths directly agree with the switch duty cycles t_n/T_s , this model is a perfect match of the pulse pattern as given by fig. 2. Moreover in this case it is valid for the entire range of one fundamental period. The intersections of the line $y = x/p$ with the modulation waveforms $x = \pi/2 ((2n+1) \pm \cos(\omega t))$ indicate a pulse transition of $i_L(\omega t)$. Here p is the carrier ratio ($p = \omega_c/\omega$), ω_c is the carrier angular frequency and ω is the fundamental angular frequency. For illustration purposes the most simple case was chosen: a sinusoidal modulation waveform along with natural sampling. The modulation waveforms are symmetrically arranged around lines of multiples of π to realise a model that supports a triangular carrier wave shape. As the widths of the resulting pulses are equal to the switching duty cycles of one semiconductor switch and the instantaneous value of the corresponding phase current is assigned to their height, these pulses resemble the outline of one of the switch currents i_{V1} , i_{V2} , i_{V3} consequently. These currents solely differ from each other by the phase shift of the respective modulation function and phase current. Evidently the sum $i_{V1} + i_{V2} + i_{V3}$ of all instantaneous valve currents finally delivers the instantaneous dc bus current value $i_{d,conv}$.

It should be remarked that by applying this method even the influence of any other PWM inverter that is connected to the dc bus can be taken into account by simply adding its current portions to the foregoing sum.

B. Evolution of the Double Fourier Series

As the wall pattern is periodic in 2π for both axes, the pulse function $F(x, y)$ may be expressed as a double Fourier series (1).

$$F(x, y) = \frac{A_{00}}{2} + \sum_{n=1}^{\infty} [A_{0n} \cos(ny) + B_{0n} \sin(ny)] + \sum_{m=1}^{\infty} [A_{m0} \cos(mx) + B_{m0} \sin(mx)] + \sum_{m=1}^{\infty} \sum_{n=1}^{\infty} [A_{mn} \cos(mx + ny) + B_{mn} \sin(mx + ny)] \quad (1)$$

$$C_{mn} = A_{mn} + jB_{mn} = \frac{1}{2\pi^2} \int_0^{2\pi} \int_0^{2\pi} F(x, y) \cdot e^{j(mx+ny)} dx dy \quad (2)$$

Where the complex Fourier coefficients can be determined with the double integral (2), see [7] - [9].

C. Derivation of DC Link and Capacitor Current Harmonics

For all upcoming calculus natural sampling is assumed which is similar to regular sampling as long as a sufficiently high carrier ratio p is assumed. Furthermore a high carrier ratio ($p > 20$) is presumed to satisfy the claim that carrier side band interference can be neglected. For the example of natural sampled modulation with a triangular carrier like shown in fig. 3 the actual complex Fourier coefficients $^{mn}i_{V1}$ of switch current i_{V1} would be identified by (3) which is derived from (2). However a modulation waveform combined with a saw tooth carrier with a trailing edge requires a term like (4).

$$^{mn}i_{V1} = \frac{\hat{i}_L}{2\pi^2} \int_0^{2\pi} \left(\int_{\frac{\pi}{2}(1-M(y))}^{\frac{\pi}{2}(3+M(y))} \cos(y - \varphi) \cdot e^{j(mx+ny)} dx \right) dy \quad (3)$$

$$^{mn}i_{V1} = \frac{\hat{i}_L}{2\pi^2} \int_0^{2\pi} \left(\int_0^{\pi(1+M(y))} \cos(y - \varphi) \cdot e^{j(mx+ny)} dx \right) dy \quad (4)$$

Equations (5) through (7) render the modulation waveforms for three most common PWM strategies as discussed here.

$$M(\omega t) = M \cdot \cos(\omega t) \quad (5)$$

$$M(\omega t) = \begin{cases} \frac{\sqrt{3}}{2} \cdot M \cdot \cos\left(\omega t - \frac{\pi}{6}\right) & \text{for } 0 < \omega t < \frac{\pi}{3} \\ & \text{or } \pi < \omega t < \frac{4\pi}{3} \\ \frac{3}{2} \cdot M \cdot \cos(\omega t) & \text{for } \frac{\pi}{3} < \omega t < \frac{2\pi}{3} \\ & \text{or } \frac{4\pi}{3} < \omega t < \frac{5\pi}{3} \\ \frac{\sqrt{3}}{2} \cdot M \cdot \cos\left(\omega t + \frac{\pi}{6}\right) & \text{for } \frac{2\pi}{3} < \omega t < \pi \\ & \text{or } \frac{5\pi}{3} < \omega t < 2\pi \end{cases} \quad (6)$$

$$M(\omega t) = \begin{cases} 1 & \text{for } -\frac{\pi}{6} < \omega t < \frac{\pi}{6} \\ \sqrt{3} \cdot M \cdot \cos\left(\omega t - \frac{\pi}{6}\right) - 1 & \text{for } \frac{\pi}{6} < \omega t < \frac{\pi}{2} \\ \sqrt{3} \cdot M \cdot \cos\left(\omega t + \frac{\pi}{6}\right) + 1 & \text{for } \frac{\pi}{2} < \omega t < \frac{5\pi}{6} \\ -1 & \text{for } \frac{5\pi}{6} < \omega t < \frac{7\pi}{6} \\ \sqrt{3} \cdot M \cdot \cos\left(\omega t - \frac{\pi}{6}\right) + 1 & \text{for } \frac{7\pi}{6} < \omega t < \frac{3\pi}{2} \\ \sqrt{3} \cdot M \cdot \cos\left(\omega t + \frac{\pi}{6}\right) - 1 & \text{for } \frac{3\pi}{2} < \omega t < \frac{11\pi}{6} \end{cases} \quad (7)$$

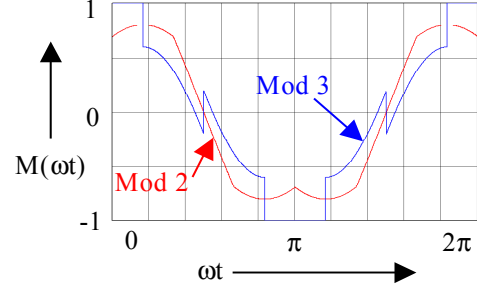


Figure 4. The modulation waveforms Mod 2 (space vector with equal zero space vector utilization) and Mod 3 (discontinuous modulation waveform) at a modulation index of $M = 1$ each

The most simple modulation function which is the cosine function (5) will be designated as Mod 1 from now on. The modulation function that is constituted by the well known space vector PWM with equal utilization of zero space vectors (6) will be denoted as Mod 2. A representative discontinuous modulation function is given by (7) and will be related to as Mod 3 in the following analysis. It would cause least switching losses at a power factor of unity. Hence it can be considered somewhat comparable to the other modulation functions as long as a phase shift of $\varphi = 0$ is considered. To preserve clarity the modulation waveforms Mod 2 and Mod 3 are depicted in fig. 4 as they appear over one fundamental period.

Obviously only the boundaries of the inner integral term of equations (3) and (4) are affected by the choice of different modulation strategies. Hence the Fourier coefficients of the switch current $^{mn}i_V$ caused by any other modulation waveform can be determined accordingly. The results of these expressions can be interpreted like this: The index m indicates the m^{th} carrier frequency band while the index n marks the n^{th} multiple of the fundamental frequency starting with $m = 0$ and with $n = -\infty \dots +\infty$ from each multiple of the carrier frequency on. Here as a precondition the magnitude of the index n is confined to half the carrier ratio unless side band interference is accounted for.

Equation (3) has been exemplary dissolved for the most simple case that is a cosine modulation function, see the appendix. It can be solved for the other modulation waveforms as well by applying the appropriate identities given in [9].

As mentioned already the dc bus current is the result of superposition of all three switch currents in the upper part of the bridge. Hence the Fourier coefficients of the dc link current are the sum of all complex Fourier coefficients describing the valve currents in the upper bridge (8).

$$^{mn}i_C = ^{mn}i_{V1} + ^{mn}i_{V2} + ^{mn}i_{V3} \quad (8)$$

IV. CALCULATION AND MEASUREMENT RESULTS OF DC LINK CURRENT HARMONICS

A. Analytical Results

Calculations of the dc link harmonics were carried out by means of the double Fourier series for all three modulation strategies along with a triangular carrier waveform each. The outcomes are presented in the diagrams of fig. 5 through 7. The peak values of the

capacitor current harmonics v_{iC} are standardized with the peak value of the ac current fundamental i_L and the frequency f is scaled by multiples of the carrier frequency f_c . The derived formulas have been evaluated with MathcadTM. The power factor was set to $\cos(\varphi) = 1$ for all calculations. A carrier ratio of $p = 60$ was assumed and the side band sequences were confined to 40 elements each. It should be pointed out that all spectra of discontinuous modulation waveforms look somewhat similar. But the one selected here ensures minimum switching losses for the presumed power factor [9]. Plotting the spectra at discrete values of the modulation index ($M = 0.1, 0.2 \dots 1.1$) results in a significant step form.

When comparing the harmonic performance of the different modulation functions it is striking that for the discontinuous one Mod 3 even when a triangular carrier is applied the first carrier frequency band still is occupied by a significant bunch of spectral lines. This also applies for the cosine modulation function in an alleviated manner as the modulation index increases (unfortunately not visible from this perspective, see also fig. 8, 11). In terms of dc link voltage harmonics reduction the modulation method Mod 2 seems to be favorable as already stated in [2].

B. Measurement Results

Measurements were taken from a voltage source converter as depicted in fig. 1 with a rated power of 22 kW and operated with a dc link voltage of $V_{dc} = 500$ V. A passive three phase ac load of $R_L = 15 \Omega$ in series with a filter inductance of $L_F = 4.5$ mH was installed at the ac terminals which causes a phase shift of $\varphi = 5.3^\circ$ at an applied fundamental frequency of $f = 50$ Hz. Thus it yields a power factor $\cos(\varphi)$ of almost unity. The switching (carrier) frequency f_c was set to 3 kHz and the modulation index was assigned to $M = 1$. Compliant to the analytical considerations the dc bus was fed by a diode bridge to deliver a well smoothed dc load current $i_{d,load}$. The dc bus current was measured for steady state operation by a current probe. The current measurements were sampled and plotted with an ONO SOKKI CF-5210 FFT analyzer. The data evaluation including the Fourier analysis was done using MatlabTM.

Once again the modulation waveforms shown in fig. 4 were compared along with a triangle carrier wave shape each. Fig. 11 - 13 show the measured counterparts of the calculated spectra in fig. 8 - 10. The measured and calculated values correspond quite well. Remaining little deviations originate from the experiment premises being slightly different to the ideal assumptions. For instance the ac line current does not possess an exact pure sinusoidal trajectory and the phase shift is slightly different from $\varphi = 0^\circ$ as initially calculated which actually is a solely theoretical operating point because a filtered line current that would converge to a pure sinusoid is only achieved with a corresponding phase shift. Another source of deviation is that instead of natural sampling that was assumed for the calculations the actual converter was operated with regular sampled PWM. The latter problem can be overcome by little modification of the presented calculation methods [9]. Furthermore breakup errors of the Fourier analysis or deviations of the pulse rate from an integer value can influence the measurement accuracy.

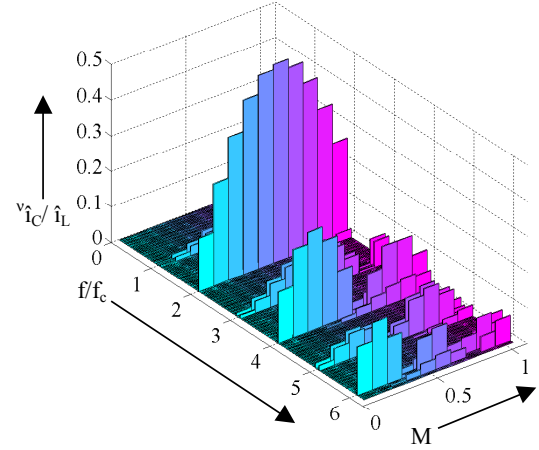


Figure 5. The calculated dc link current spectra for Mod 1 (cosine modulation waveform) combined with a triangular carrier function, $\varphi = 0$

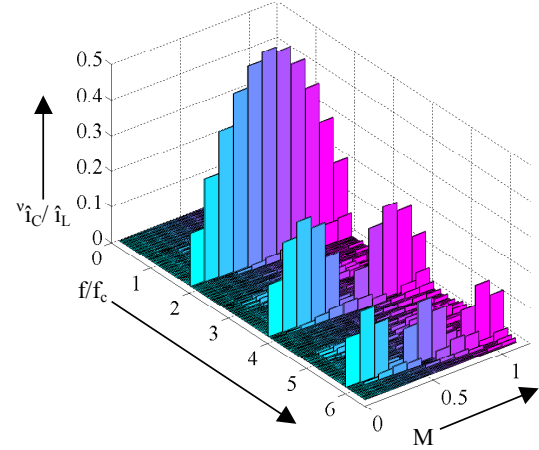


Figure 6. The calculated dc link current spectra for the spectra for Mod 2 (space vector modulation with equal utilization of zero space vectors) combined with a triangular carrier function, $\varphi = 0$

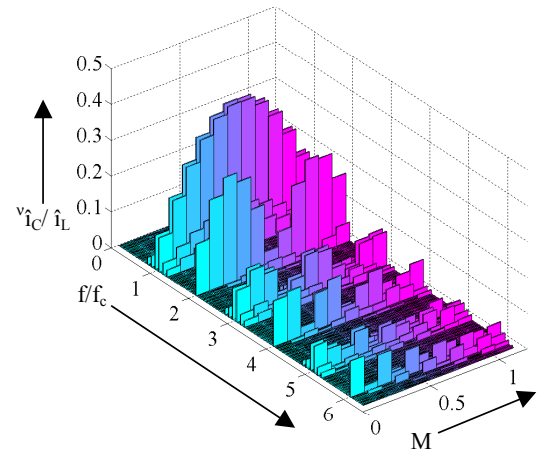


Figure 7. The calculated dc link current spectra for Mod 3 (discontinuous modulation waveform) combined with a triangular carrier function, $\varphi = 0$

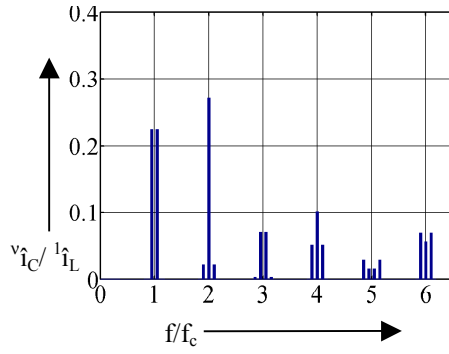


Figure 8. The calculated dc link current spectra for Mod 1 (cosine modulation waveform) combined with a triangular carrier function, $M = 1$, $\varphi = 0$

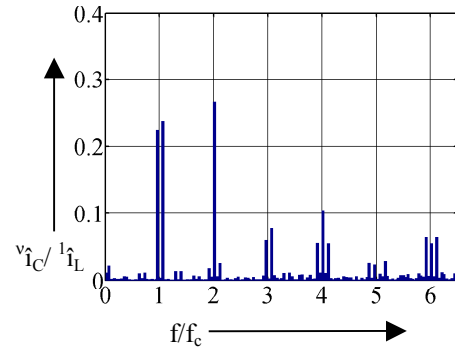


Figure 11. The measured dc link current spectra for Mod 1 (cosine modulation waveform) combined with a triangular carrier function, $M = 1$, $\varphi = 5^\circ$

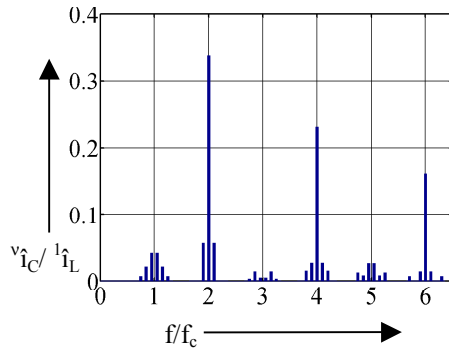


Figure 9. The calculated dc link current spectra for Mod 2 (space vector modulation with equal utilization of zero space vectors) combined with a triangular carrier function, $M = 1$, $\varphi = 0$

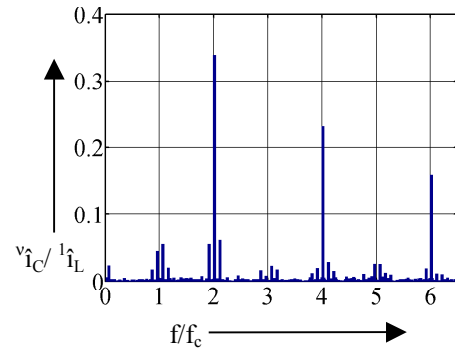


Figure 12. The measured dc link current spectra for Mod 2 (space vector modulation with equal utilization of zero space vectors) combined with a triangular carrier function, $M = 1$, $\varphi = 5^\circ$

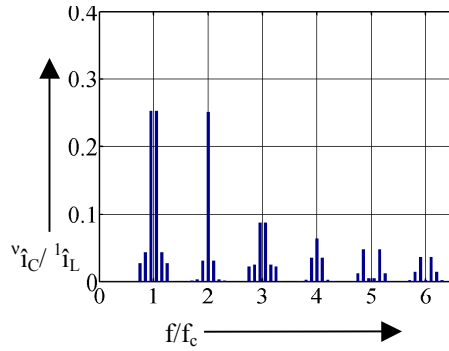


Figure 10. The calculated dc link current spectra for Mod 3 (discontinuous modulation waveform according to fig. 4) combined with a triangular carrier function, $M = 1$, $\varphi = 0$

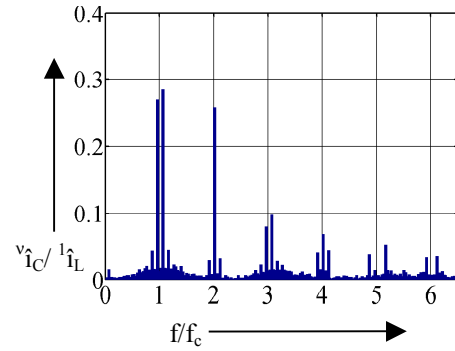


Figure 13. The measured dc link current spectra for Mod 3 (discontinuous modulation waveform according to fig. 4) combined with a triangular carrier function, $M = 1$, $\varphi = 5^\circ$

V. CONCLUSION

A new method for the calculation of dc link current harmonics for voltage source converters operated by any modulation strategy is presented.

As means of analysis the geometric wall model approach for the determination of double Fourier series describing the dc link current harmonics is proposed and applied to three selected cases. With this method it is feasible to determine the dc bus current spectra for all kinds of modulation strategies with moderate effort. Moreover it gives the opportunity to account for further converters that are connected to the same dc bus as long as

the phase shift of the resulting harmonics is regarded carefully.

Results of dc link current spectra calculated by means of this method and their comparison are presented. They render information on the dc bus current spectra dispersion and thereby on the predominant influence of the modulation strategy. Different exemplary modulation functions are investigated and compared, continuous and discontinuous ones along with a triangle carrier each. The theoretical outcomes are proved by additional measurements. The presented method contributes to detailed dc bus capacitor sizing as it facilitates the prediction of the dc bus current spectra for any kind of modulation method.

REFERENCES

- [1] J.W. Kolar, H. Ertl, F.C. Zach, "Calculation of the passive and active component stress of three phase PWM converter systems with high pulse rate," *EPE 89*, vol. 3, pp. 1303–1311, 1989.
- [2] P.A. Dahono, Y. Sato, T. Kataoka, "Analysis and minimization of Ripple components of input current and voltage of PWM inverters", *IEEE Trans. on Ind. App.*, vol. 32, No.4, July/August 1996
- [3] F. Renken, "Analytic calculation of the dc-link capacitor current for pulsed three phase inverters", *EPE-PEMC 04*, Riga, CD ROM article, 2004
- [4] M. Winkelkemper, S. Bernet, "Design and optimization of the dc-link capacitor of PWM voltage source inverter with active frontend for low-voltage drives", *EPE 03*, Toulouse, CD ROM article, 2003
- [5] F.D. Kieferndorf, M. Förster, T.A. Lipo, "Reduction of dc bus capacitor ripple current with PAM/PWM converter" *EPE 03*, Toulouse, CD ROM article, 2003
- [6] M.L. Gasperi, "A method for predicting the expected life of bus capacitors", *IEEE Industry Applications Society Annual Meeting*, vol.2, pp. 1042-1047, 1997
- [7] H.S. Black, *Modulation Theory*, Van Nostrand, 1953
- [8] J.F. Moynihan, M.G. Egan, J.M.D. Murphy, "Theoretical spectra of space-vector-modulated waveforms", *IEE Proc.-Electr. Power Appl.*, Vol. 145, No. 1, January 1998
- [9] D.G. Holmes, T.A. Lipo, *Pulse width modulation for power converters*, IEEE press series on power engineering, Piscataway, 2003
- [10] K. Zhou, D. Wang, "Relationship between space-vector modulation and three-phase carrier based PWM: a comprehensive analysis", *IEEE Trans. on Ind. Electr.*, vol. 49, No.1, February 2002
- [11] F. Jenni, D. Wüest, *Steuerverfahren für Selbstgeführte Stromrichter*, B. G. Teubner, Stuttgart, 1995

APPENDIX

As an example the following chapter presents the dissolution of (3) for a cosine modulation waveform (5). As such (3) can also be written as (10) with (9).

$$\cos(\alpha) = \frac{1}{2} \cdot (e^{j\alpha} + e^{-j\alpha}) \quad (9)$$

$$\begin{aligned} {}^{mn}i_{V1} = & \frac{\hat{i}_L}{j4\pi^2 m} \left[e^{j\left(m\frac{3\pi}{2}-\varphi\right)} \int_0^{2\pi} e^{j(n+1)y} \cdot e^{j\left(m\frac{\pi}{2}M \cdot \cos(y)\right)} dy \right. \\ & - e^{j\left(m\frac{\pi}{2}-\varphi\right)} \int_0^{2\pi} e^{j(n+1)y} \cdot e^{j\left(-m\frac{\pi}{2}M \cdot \cos(y)\right)} dy \\ & + e^{j\left(m\frac{3\pi}{2}+\varphi\right)} \int_0^{2\pi} e^{j(n-1)y} \cdot e^{j\left(m\frac{\pi}{2}M \cdot \cos(y)\right)} dy \\ & \left. - e^{j\left(m\frac{\pi}{2}+\varphi\right)} \int_0^{2\pi} e^{j(n-1)y} \cdot e^{j\left(-m\frac{\pi}{2}M \cdot \cos(y)\right)} dy \right] \quad (10) \end{aligned}$$

With the identity given by (11), see also [7], (10) can be turned into (12) comprising Bessel functions of first kind and n^{th} order.

$$J_n(Z) = \frac{j^{-n}}{2\pi} \cdot \int_0^{2\pi} e^{jZ \cdot \cos(\alpha)} e^{jn\alpha} d\alpha \quad (11)$$

$$\begin{aligned} {}^{mn}i_{V1} = & \frac{\hat{i}_L \cdot j^n}{2\pi \cdot m} \left[e^{j\left(m\frac{3\pi}{2}-\varphi\right)} \cdot J_{n+1}\left(m\frac{\pi}{2} \cdot M\right) \right. \\ & - e^{j\left(m\frac{\pi}{2}-\varphi\right)} \cdot J_{n+1}\left(-m\frac{\pi}{2} \cdot M\right) \\ & + e^{j\left(m\frac{3\pi}{2}+\varphi\right)} \cdot J_{n-1}\left(m\frac{\pi}{2} \cdot M\right) \\ & \left. - e^{j\left(m\frac{\pi}{2}+\varphi\right)} \cdot J_{n-1}\left(-m\frac{\pi}{2} \cdot M\right) \right] \quad (12) \end{aligned}$$

for $n = -\infty \dots +\infty$ and $m = 1, 2, \dots$

As can be seen above the case for $m = 0$ cannot be regarded by (12). Thus a distinction of cases yields (13) as deduced from (3).

$${}^{0n}i_{V1} = \frac{\hat{i}_L}{j2\pi^2} \int_0^{2\pi} e^{jn \cdot y} (\pi + \pi \cdot M \cdot \cos(y)) \cdot \cos(y - \varphi) dy \quad (13)$$

It turns out that after employing l'Hospital's rule on (13) there are only values remaining for $n = 0, 1, 2$ as can be seen by (14).

$${}^{0n}i_{V1} = \begin{cases} \frac{M \cdot \hat{i}_L}{j \cdot 2} \cdot \cos(\varphi) & \text{if } n = 0 \\ \frac{\hat{i}_L}{j \cdot 2} \cdot e^{j\varphi} & \text{if } n = 1 \\ \frac{M \cdot \hat{i}_L}{j \cdot 4} \cdot e^{j\varphi} & \text{if } n = 2 \end{cases} \quad (14)$$